ISSN 1560-0904, Polymer Science, Series B, 2017, Vol. 59, No. 1, pp. 109–116. © Pleiades Publishing, Ltd., 2017.

COMPOSITES

Polystyrene/Mesoporous Diatomite Composites by in situ Simultaneous Reverse and Normal Initiation Technique for Atom Transfer Radical Polymerization[1]

Khezrollah Khezri[a] and Yousef Fazli[b,*]

[a] *Young Researchers and Elites Club, Central Tehran Branch, Islamic Azad University, Tehran, Iran*
[b] *Department of Chemistry, Faculty of Science, Arak Branch, Islamic Azad University, Arak, Iran*
**e-mail: y-fazli@iau-arak.ac.ir, yousef.fazli75@gmail.com*

Received June 20, 2016;
Revised Manuscript Received August 22, 2016

Abstract– Mesoporous diatomite platelets were employed to synthesize different polystyrene/diatomite composites by in situ polymerization of styrene via simultaneous reverse and normal techniques of atom transfer radical polymerization. Furrier transform infrared spectroscopy, thermogravimetric analysis, differential scanning calorimetry, scanning and transmission electron microscopy, gas and size exclusion chromatography were used to examine characteristics of polymer and composite. Addition of 3 wt% pristine mesoporous diatomite leads to increase of conversion from 79 to 93%, while control over molecular weight characteristics become worse.

DOI: 10.1134/S1560090417010092

INTRODUCTION

The field of polymer based nanocomposites has been greatly recognized as one of the most interesting and rapidly emerging research areas in materials chemistry [1, 2]. Nanocomposites are comprised from suitable combination of two or more nanofillers with an organic polymer matrix in which can combine the advantages of inorganic nanofillers (e.g. rigidity and thermal stability) and the organic polymers (e.g. flexibility and processability) [3]. Relatively low-volume addition (1–10%) of inorganic nanofillers such as alumina, MCM-41, and clay platelets into the polymer matrix results in considerable enhancement in several properties such as thermal and mechanical properties, fire retardance, and gas barrier property in comparison with virgin common polymers or conventionally filled composites [4, 5]. Unique properties of the nanofillers as a reinforcing agent can be attributed to their high aspect ratio. According to the fact that how many dimensions of the dispersed nanofillers are in the nanometer range, nanocomposites can be classified into three groups: nanocomposites with 3D fillers (e.g. silica nanoparticles), nanocomposites with 2D fillers (e.g. whiskers), and nanocomposites with 1D fillers (e.g. clay) [6].

Among different methods for the preparation of nanocomposites including in situ polymerization, solution and melt intercalation, in situ polymerization is more common and facilitate [7]. Synthesis of well-defined polymer chains with desired functionalities, architectures, and composition as an organic phase of nanocomposites has attracted great attention during the last decades [8].

Diatomite as a nature-designed nanomaterial is mainly made up by nonconductive non-crystal silicon dioxide ($SiO_2 \cdot nH_2O$) [9]. Diatomite is pale-colored, soft, and light-weight sedimentary rock composed principally of silica microfossils of single-cell photosynthetic algae (Diatoms) [10]. Diatomite possesses specific physical and chemical properties that make it a suitable candidate for many applications. Highly porous structure (porosity up to 80%), low thermal conductivity, low density, chemical inertness and high absorption capacity are some unique characteristics features of diatomite [11, 12]. Diatomaceous earth mineral or kieselgur can be provided in large quantities with low cost and therefore it can be considered as an inexpensive biomaterial with nanoscale three-dimensions offering enormous perspectives for the development of new materials [13]. Because of these unique features of diatomite, it can be applied in a wide variety of applications and research fields: support in the reactions, sound and heat insulation, water treatment, removal processes, manufacture of explosives and as filters [14, 15].

[1] The article is published in the original.

Anionic and cationic polymerization, ring-opening metathesis, and group transfer radical polymerization are some living polymerization procedures that can be employed to the synthesis of well-defined polymers with controlled molecular weight and low polydispersity index (PDI) [16]. Although by these methods the majority deficiencies of free radical polymerization are circumvented (such as control over the molecular weight, PDI, synthesis of pure block copolymers), requirement of drastic experimental conditions and high sensitivity to impurities (air and moisture) are some important deficiencies of these methods [17]. Introducing of reversible deactivation radical polymerization (RDRP) methods provide appropriate pathways to combine the useful advantages of conventional radical polymerization (application of wide variety of monomers, wide range of reaction temperatures, and different polymerization systems and media) and living polymerization processes (synthesis of tailor-made polymers) [16, 18]. Although different methods for RDRP are proposed, the most successful methods include stable free-radical mediated polymerization [19], atom transfer radical polymerization (ATRP) [20], and reversible addition–fragmentation chain transfer polymerization [21]. Among them, ATRP presents some unique advantages over other; commercial availability of its reagents (ligands, alkyl halides, and transition metals), mild polymerization conditions, remarkable tolerance to different functional groups, great industrialization prospects [16, 22].

A review of literatures indicates that there is not an obvious research on the application of diatomite as filler to synthesize polymer/diatomite composites. However, Karaman et al. have prepared polyethylene glycol (PEG)/diatomite composite as a novel form-stable composite phase change material (PCM), in which the PCM was prepared by incorporating PEG in the pores of diatomite [23]. Li et al. have synthesized conducting diatomite by polyaniline on the surface of diatomite. Linkage of polyaniline on the surface of diatomite is attributed to the hydrogen bond between the surface of diatomite and polyaniline macromolecules [24]. Li et al. have also prepared fibrillar polyaniline/diatomite composite by one-step in situ polymerization. According to their results, the polyaniline/diatomite composite can be applied as fillers for electromagnetic shielding materials and conductive coatings [25]. In addition, other studies such as investigating the effects of extrusion conditions on die-swell behavior of polypropylene/diatomite composite melts and crystallization behaviors and foaming properties of diatomite-filled polypropylene composites have been performed [26, 27].

In this research, simultaneous reverse and normal initiation technique for atom transfer radical polymerization (SR&NI ATRP) of styrene in the presence of pristine diatomite nanoplatelets is investigated. This technique is selected for its attractive features; application of transition metal complex in its high oxidation state, and decrement of metal concentration in the final products. Effect of pristine diatomite nanoparticles on conversion, molecular weights, and PDI values of the synthesized composites by in situ SR&NI ATRP and thermal properties of the products are discussed in detail.

EXPERIMENTAL

Materials

Diatomite earth sample was obtained from Kamel Abad-Azerbaijan-I.R. Iran. It was dispersed in 100 mL distilled water by magnetic stirring and then it was kept constant until some solid impurities were dispersed. The particles were separated with filter paper and dried at 100°C for 8 h. Styrene (St, Aldrich, 99%) was passed through an alumina-filled column, dried over calcium hydride, and distilled under reduced pressure (60°C, 40 mm Hg). Copper(II) bromide ($CuBr_2$, Fluka, 99%), *N*,*N*,*N*′,*N*″,*N*‴-pentamethyldiethylenetriamine (PMDETA, Aldrich, 99%), ethyl alpha-bromoisobutyrate (EBiB, Aldrich, 97%), 2,2′–azobisisobutyronitrile (AIBN, Acros), anisole (Aldrich, 99%), tetrahydrofuran (THF, Merck, 99%), and neutral aluminum oxide (Aldrich, 99%) were used as received.

Preparation of Polystyrene/Diatomite Nanocomposite by in situ SR&NI ATRP

First SR&NI ATRP of styrene was performed in a 200 mL three-neck lab reactor equipped with a reflux condenser, nitrogen inlet valve, and a magnetic stir bar that was placed in an oil bath. A typical batch of polymerization was run at 110°C with the molar ratio of 150 : 1 : 0.2 : 0.2 : 0.12 for [Styrene] : [EBiB] : [$CuBr_2$] : [PMDETA] : [AIBN] giving a theoretical polystyrene molecular weight of $M_n = 15.6 \times 10^3$ at final conversion. At first, styrene (15 mL), $CuBr_2$ (0.052 g, 0.23 mmol), PMDETA (0.04 mL, 0.23 mmol) and anisole (7 mL) were added to the reactor. Then, it was degassed and back-filled with nitrogen three times, and then left under N_2 with stirring at room temperature. The solution turned green color as the $CuBr_2$/PMDETA complex was formed. When the majority of the metal complex had formed, reaction temperature was increased to 110°C during 10 min. Subsequently, predeoxygenated solution of AIBN (0.023 g, 0.13 mmol) in the styrene (5 mL) and predeoxygenated EBiB (0.17 mL, 1.16 mmol) were injected into the reactor to start the polymerization reaction. At the beginning of the reaction, polymerization media was green and gradually changed to brown. Samples were taken at the end of the reaction to measure the final conversion.

Table 1. Designation of the samples

Sample	Method of preparation	Proportion of pristine diatomite nanoplatelets, wt %	Dispersion time prior to the polymerization, h
PPS	SR&NI ATRP	0	–
PSDC 1	*In situ* SR&NI ATRP	1	19
PSDC 2	*In situ* SR&NI ATRP	2	19
PSDC 3	*In situ* SR&NI ATRP	3	19

For preparation of nanocomposites, a desired amount of pristine diatomite nanoplatelets was dispersed in 10 mL of styrene and the mixture was stirred for 19 h. Then, the remained 5 mL of styrene was added to the mixture. Subsequently, polymerization procedure was applied accordingly. In the samples designation, PPS refers to the neat polystyrene and PSDC X implies different nanocomposites with X percentages of pristine diatomite nanoplatelets loading. Table 1 presents designation of the samples with the percentage of pristine diatomite nanoplatelets.

For separating of polystyrene chains from pristine diatomite nanoplatelets, nanocomposites were dissolved in THF. By high-speed ultracentrifugation (10^4 rpm) and then passing the solution through a 0.2 micrometer filter, polystyrene chains were separated from pristine diatomite nanoplatelets. Subsequently, polymer solutions passed through an alumina column to remove catalyst species.

Characterization

FTIR spectrum of the pristine diatomite nanoplatelets was recorded using a Bruker FTIR spectrophotometer, within a range of 400–4400 cm^{-1}. Materials porosity was characterized by N_2 adsorption/desorption curves obtained with a Quntasurb QS18 (Quntachrom) apparatus. The surface area and pore size distribution values were obtained with the corrected BET equation (Brunauer–Emmett–Teller). In addition, specific surface area measurements were also performed with an NS-93 apparatus (Towse-e-Hesgarsazan Asia, Iran). Pore size distributions were also calculated by the Barrett–Joyner–Halenda (BJH) method. Surface morphology of the pristine diatomite was examined by SEM (Philips XL30) with acceleration voltage of 20 kV. The transmission electron microscope, Philips EM 208 (The Netherlands), with an accelerating voltage of 120 kV was employed to study the morphology of the pristine diatomite nanoplatelets. The specimens were prepared by coating a thin layer on a mica surface using a spin coater (Modern Technology Development Institute, Iran). Gas chromatography (GC) is a simple and highly sensitive characterization method and does not require removal of the metal catalyst particles. GC was performed on an Agilent-6890N with a split/splitless injector and flame ionization detector, using a 60 m HP-INNO-WAX capillary column for the separation. The GC temperature profile included an initial steady heating at 60°C for 10 min and a 10 deg/min ramp from 60 to 160°C. The samples were also diluted with acetone. The ratio of monomer to anisole was measured by GC to calculate monomer conversion throughout the reaction. Size exclusion chromatography (SEC) was used to measure the molecular weight and molecular weight distribution. A Waters 2000 ALLIANCE with a set of three columns of pore sizes of 10^4, 10^3, and 500 Å was utilized to determine polymer average molecular weight and polydispersity index (PDI). THF was used as the eluent at a flow rate of 1.0 mL/min, and calibration was carried out using low polydispersity polystyrene standards. Thermal gravimetric analysis (TGA) was carried out with a PL thermo-gravimetric analyzer (Polymer Laboratories, TGA 1000, UK). Thermograms were obtained from ambient temperature to 700°C at a heating rate of 10 deg/min. Thermal analysis were carried out using a differential scanning calorimetry (DSC) instrument (NETZSCH DSC 200 F3, Netzsch Co, Selb/Bavaria, Germany). Nitrogen at a rate of 50 mL/min was used as purging gas. Aluminum pans containing 2–3 mg of the samples were sealed using DSC sample press. The samples were heated from ambient temperature to 220°C at a heating rate of 10 deg/min.

RESULTS AND DISCUSSION

Since inherent characteristics of the pristine diatomite nanoplatelets can affect the kinetics of in situ polymerization and consequently nanocomposite properties, these characteristics are evaluated.

FTIR spectrum of the pristine diatomite nanoplatelets is presented in Fig. 1. The bands at 3434 and 1634 cm^{-1} correspond to the stretching vibrations of physically adsorbed water and zeolitic water, respectively [28]. Although the diatomite sample is rehydrated, during the preparation process and obtaining the spectrum some water molecules may be re-adsorbed [29]. The strong band at 1098 cm^{-1} is attributed to the stretching mode of siloxane (Si–O–Si). In addition, the band at 471 cm^{-1} is associated

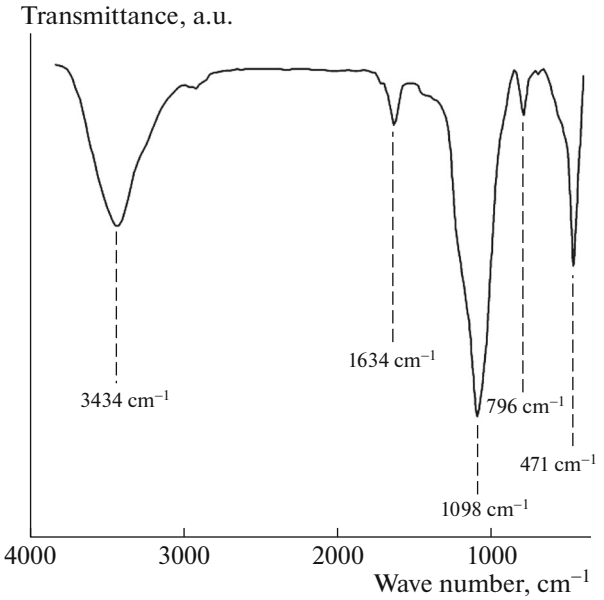

Fig. 1. FTIR spectrum of the pristine diatomite nanoplatelets.

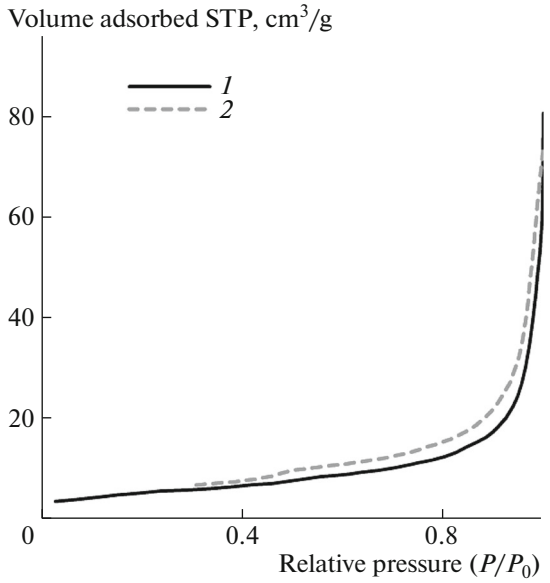

Fig. 2. Nitrogen (*1*) adsorption and (*2*) desorption isotherm of the pristine diatomite nanoplatelets.

with the asymmetric stretching mode of siloxane bonds. The band at 796 cm^{-1} is also attributed to the vibration of O–H [28].

Figure 2 represents nitrogen adsorption/desorption isotherms of the pristine diatomite nanoplatelets. The shape of isotherm is similar to the IV type isotherms according to the IUPAC classification and confirms that diatomite has mesoporous structure. The hysteresis is associated with the filling and emptying of the mesopores by capillary condensation [30]. A sharp increase in the nitrogen adsorbed quantity near the relative pressure equal to 1 demonstrates the existence of macropores in the pure diatomite and therefore non-uniform pore size distribution can be comprehended [31].

Extracted data from the nitrogen adsorption/desorption isotherm are summarized in Table 2.

According to TGA data, two main mass losses are observed. The first mass loss is mainly ascribed to the dehydration of diatomite (the weight loss below 150°C is due to the removal of physisorbed water whilst the weight loss at 150–300°C can be attributed to the expulsion of chemisorbed water molecules). The second weight loss in the temperature range of 400–700°C is a gradual and slow loss and may be associated with the dehydroxylation of the silanols of diatomite. Pristine diatomite nanoparticles leave 92.3% char at 700°C.

Figure 3 presents SEM (a) and TEM (b) images of the pristine diatomite nanoplatelets. Pristine diatomite nanoplatelets are composed of plaque plate particles with spherical-shaped pores. These plates have regular pores and sometimes are aggregated. This unique structure is suitable for the synthesis of various nanocomposites and makes it as an appropriate catalyst support. According to TEM image, pristine diatomite nanoplatelets belong numerous regularly spaced rows of pores in its structure that this observation is confirmed with SEM images. In addition, average pore diameter from TEM images is estimated between 33–40 nm.

Among different ATRP techniques, SR&NI ATRP is employed since it provides a robust route to circumvent oxidation problems (application of transition metal complex in its high oxidation state). Moreover, despite reverse ATRP, SR&NI ATRP results in lower metal concentration in the final products. According to the Scheme 1, SR&NI ATRP employs a dual initiator system consisting of free radical initiator (e.g.

Table 2. Extracted data from nitrogen adsorption/desorption isotherm of the pristine diatomite nanoplatelets

BET surface area	Langmuir surface area	Average pore diameter (4V/A by BET)	BJH Plot $d_{p,\,peak}$ (Area)	
			Adsorption branch	Desorption branch
19.05 m^2/g	28.06 m^2/g	24.27 nm	4.19 nm	3.72 nm

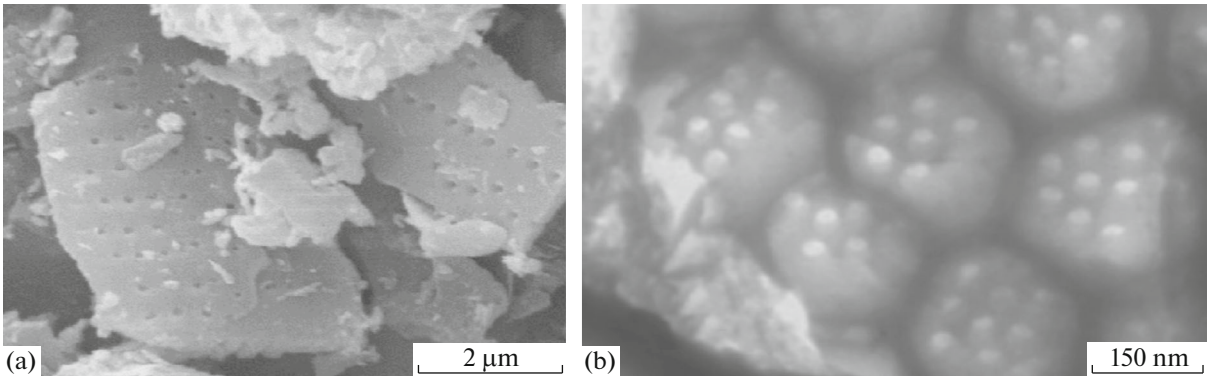

Fig. 3. (a) SEM and (b) TEM images of the pristine diatomite nanoplatelets.

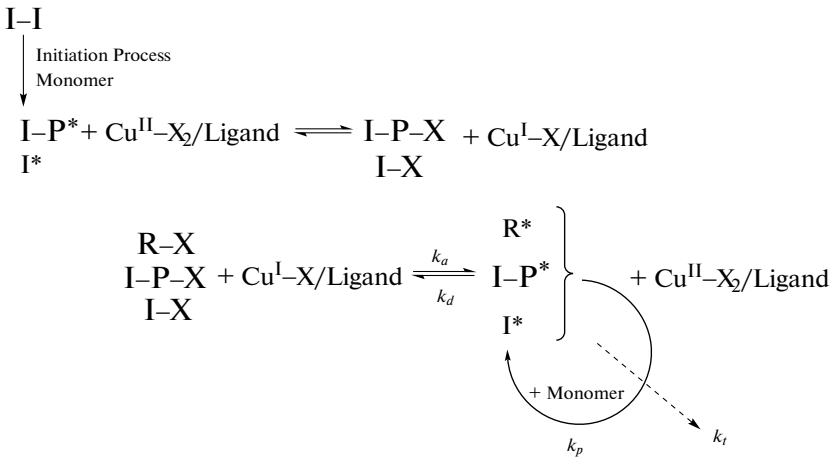

Scheme 1.

AIBN) and alkyl halide (e.g. EBiB). It starts by a reaction between CuX_2/ligand and radicals, which are generated from the radical initiator. After that, the generated CuX/ligand participates in another reaction with ATRP initiator [32]. In general, SR&NI ATRP opens a practical synthetic path to synthesize tailor-made polymers with various compositions and architectures.

It was found that SR&NI ATRP of styrene without diatomite nanoplatelets results in tailor-made polystyrene with low PDI value in combination with high conversion (Table 3). By adding pristine diatomite nanoplatelets, general equilibrium of SR&NI ATRP is disturbed, which result in increase of both conversion and PDI values. By addition of only 3 wt% of diatomite nanoplatelets, final conversion increases from 79 to 93%. Moreover, a noticeable growth of PDI values is also occurred (from 1.15 to 1.42). Positive effect of the pristine diatomite nanoplatelets on the molecular weight of the samples can be interpreted by abundant pendant hydroxyl groups of the pristine diatomite. It is demonstrated that polar solvents (especially hydroxyl containing ones, like water, phenol, and carboxylic acids) exert a rate acceleration effect on the polymerization systems for increasing radical activation rate and also reducing radical recombination rate. Numerous pendant hydroxyl groups on the surface of the pristine diatomite nanoplatelets can possibly cause a polarity change into the reaction medium. In addition, negatively charged surface (pendant hydroxyl groups on the surface of the pristine diatomite nanoplatelets) could absorb and gather positively charged catalyst (Cu ions at our work) and consequently enhances the chain growth rate. The accelerating effect of other nano-fillers such as nanoclay and MCM-41 nanoparticles on polymerization rate was also reported elsewhere [33–35]. PDI values of the polymer chains increases by the addition of pristine diatomite nanoplatelets. Diatomite nanoplatelets acts as an impurity in the polymerization medium and therefore causes the broadening of molecular weight distribution of the resultant polymers [36].

Table 3. Molecular weights and PDI values of the extracted polystyrenes resulted from SEC traces

Conversion, %	Time, h	Sample	$M_n \times 10^{-3}$		PDI
			Theory	Experiment	
PPS	10	79	12.6	12.4	1.15
PSDC 1	10	84	13.2	13.1	1.26
PSDC 2	10	87	13.4	13.6	1.34
PSDC 3	10	93	14.1	14.5	1.42

Table 4. TGA and DSC data for the neat polystyrene and its nanocomposites

Sample	Charat 650°C, %	T_g, °C
PPS	1.8	83.5
PSDC 1	3.3	87.2
PSDC 2	4.8	89.4
PSDC 3	6.3	91.3

Theoretical molecular weight is calculated by using equation:

$$M_n^{Theo} = \frac{[M]_0}{[EBiB]_0} \times Conversion \times M_{monomer},$$

where $[M]_0$ and $[EBiB]_0$ are initial concentration of the monomer and initiator, and $M_{monomer}$ represents molecular weight of styrene which is equals to 104.15 g/mol.

A suitable agreement between the theoretical and experimental molecular weights in combination with low PDI values (PDI < 1.45) can be considered as an appropriate evidences for controlled nature of the polymerization. Also, color change of the reaction media during polymerization from light green to light brown is an evidence of successful SR&NI ATRP equilibrium establishment.

Thermal stability of the neat polystyrene and its various nanocomposites is evaluated by TGA. Thermograms of weight loss as a function of temperature in the temperature range of 30–650°C are given in Fig. 4a. As is seen, thermal stability of the neat polystyrene is lower than all of the nanocomposites. In addition, thermal stability of the neat polystyrene is improved by adding diatomite nanoplatelets. Moreover, by increasing diatomite content, an increase in degradation temperatures is observed. In general, in the TGA graphs three separated steps can be identified. First step: evaporation of the water molecules results in the weight loss between 100–150°C. Second step: degradation of volatile materials such as residual monomer and low molecular weight oligomers (at the temperature window around 180–370°C). Third step: degradation of the synthesized polymer and nanocomposites (the main degradation step) is started at the temperatures around 400°C.

Degradation temperature of the samples versus amount of degradation is used to show that addition of diatomite nanoplatelets in the polymer matrix results in an improvement of thermal stabilities of the nanocomposites (Fig. 4b; T_X is the temperature threshold, at which *X*% of neat polystyrene and its nanocomposites is degraded). Char values at 650°C are also pre-

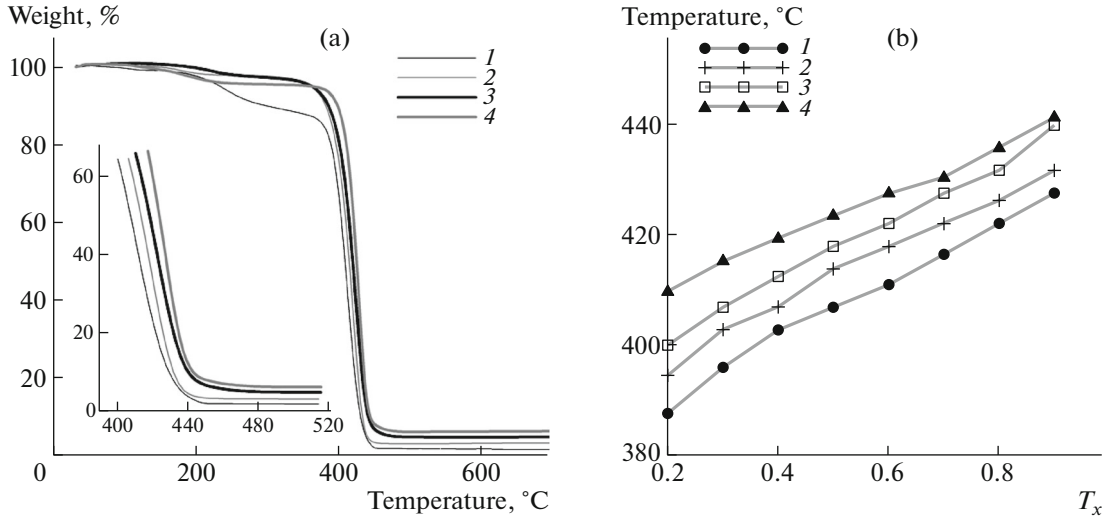

Fig. 4. (a) Thermograms of the neat polystyrene and its various nanocomposites and (b) graphical illustration of temperature and degradation relationship: (*1*) PPS, (*2*) PSDC1, (*3*) PSDC2, and (*4*) PSDC3.

sented in Table 4. As it is expected, char values increase by increasing pristine diatomite nanoplatelets loading.

Improvement of thermal stability of the nanocomposites by adding diatomite nanoplatelets content can be attributed to the high thermal stability of diatomite nanoplatelets and to interaction between diatomite platelets and polymer matrix [37]. Physical interaction between polystyrene chains and surface of the pristine diatomite nanoplatelets is an important factor for increasing thermal stability of the nanocomposites. Additionally, hindrance effect of diatomite platelets on the polymer chains movement and restriction of oxygen permeation by these sheets are the other reasons for higher thermal stability of the nanocomposites. Similar conclusions are also achieved in the case of polymer/clay nanocomposites [35, 38].

According to DSC, in the temperature range of 45–180°C no transitions for pristine diatomite nanoplatelets are observed, therefore only thermal transition of polymers can take place. In these experiments, samples are heated from room temperature to 220°C to remove their thermal history. Then, they cooled to room temperature to distinguish the phase conversion and other irreversible thermal behaviors. Finally, samples are heated from room temperature to 220°C to obtain T_g values. The structure of the synthesized polymer and its nanocomposites is amorphous and no crystallization phenomenon is observed. As is seen from Table 4, T_g value of the neat polystyrene is lower than all of the nanocomposites and an increase in pristine diatomite nanoplatelets content results in rise of T_g value. This may be attributed to the confinement effect of the diatomite nanoplatelets. The rigid two-dimensional diatomite nanoplatelets can restrict the steric mobility of polystyrene chains and cause the increase of T_g. Similar conclusions are done in the case of polymer/clay nanocomposites [35, 38].

CONCLUSIONS

In situ SR&NI ATRP of styrene was employed to synthesize well-defined polystyrene and its nanocomposites in the presence of pristine mesoporous diatomite platelets. Mesoporous structure, existence of plaque plate particles with spherical-shaped pores, silica as the main constituent, and existence of numerous regularly spaced rows in its structure are some inherent features of the pristine diatomite platelets. In situ SR&NI ATRP of styrene in the presence of pristine mesoporous diatomite leads to rise of conversion, molecular weight and PDI values. Improvement in thermal stability of the nanocomposites and increasing T_g values is also observed by incorporation of pristine mesoporous diatomite platelets.

REFERENCES

1. H. Du, G. Q. Xu, and W. S. Chin, Chem. Mater. **14**, 4473 (2002).
2. Q. Zhang, N. Hao, Q. Zhang, and Z. Liu, Polym. Sci., Ser B **57**, 522 (2015).
3. K. Khezri, H. Roghani-Mamaqani, J. Compos. Mater. **49**, 1525 (2015).
4. R. A. Vaia and J. F. Maguire, Chem. Mater. **19**, 2736 (2007).
5. K. Deng, J. Liu, X. Zheng, Y. Zhang, N. Jia, H. Tian, and Y. Liu, Polym. Adv. Technol. **19**, 1048 (2008).
6. D. W. Schaefer and R. S. Justice, Macromolecules **40**, 8501 (2007).
7. S. Varghese and J. Karger-Kocsis, Polymer **44**, 4921 (2003).
8. H. Roghani-Mamaqani, and K. Khezri, J. Polym. Res. **23**, 190 (2016).
9. W. Weiliang, Procedia Environ. Sci. **12**, 79 (2012).
10. S. Nenadovic, M. Nenadovic, R. Kovacevic, L. Matovic, B. Matovic, Z. Jovanovic, and J. Grbovic Novakovic, Sci. Sintering **41**, 309 (2009).
11. X. Li, X. Li, N. Dai, and G. Wang, Appl. Surf. Sci. **255**, 8276 (2009).
12. Y. Du, J. Yan, Q. Meng, J. Wang, and H. Dai, Mater. Chem. Phys. **133**, 907 (2012).
13. P. Yuan, D. Liu, D. Tan, K. Liu, H. Yu, Y. Zhong, A. Yuan, W. Yu, and H. He, Microporous Mesoporous Mater. **170**, 9 (2013).
14. X. Li, X. Li, and G. Wang, Mater. Chem. Phys. **102**, 140 (2007).
15. Y. Jia, W. Han, G. Xiong, and W. Yang, Sci. Technol. Adv. Mater. **8**, 106 (2007).
16. Y. Fazli, H. Alijani, and K. Khezri, Adv. Polym. Technol. **35**, 21549 (2016).
17. J. Qiu, B. Charleux, and K. Matyjaszewski, Prog. Polym. Sci. **26**, 2083 (2001).
18. P. B. Zetterlund, Y. Kagawa, and M. Okubo, Chem. Rev. **108**, 3747 (2008).
19. C. J. Hawker, A.W. Bosman, and E. Harth, Chem. Rev. **101**, 3661 (2001).
20. K. Khezri, H. Roghani-Mamaqan, M. Sarsabili, M. Sobani, and S. Mirshafiei-Langari, Polym. Sci., Ser B **56**, 909 (2014).
21. Y. Fazli, H. Alijani, and K. Khezri, J. Inorg. Organomet. Polym. **25**, 1189 (2015).
22. M. Sarsabili, K. Kalantari, and K. Khezri, J. Therm. Anal. Calorim. **126**, 1261 (2016).
23. S. Karaman, A. Karaipekli, A. Sarı, and A. Bicer, Sol. Energy Mater. Sol. Cells **95**, 1647 (2011).
24. X. Li, C. Bian, W. Chen, J. He, Z. Wang, N. Xu, and G. Xue, Appl. Surf. Sci. **207**, 378 (2003).
25. X. Li, X. Li, and G. Wang, Appl. Surf. Sci. **249**, 266 (2005).
26. S. Hu, X. Zhu, W. Hu, L. Yan, and C. Cai, Polym. Bull. **70**, 517 (2013).
27. J. Z. Liang, Polym. Test. **27**, 936 (2008).
28. G. Sheng, H. Dong, and Y. Li, J. Environ. Radioact. **113**, 108 (2012).

29. I. Rea, N. M. Martucci, L. De Stefano, I. Ruggiero, M. Terracciano, P. Dardano, N. Migliaccio, P. Arcari, R. Taté, I. Rendina, and A. Lamberti, Biochim. Biophys. Acta **1840**, 3393 (2014).
30. Z. Sun, X. Yang, G. Zhang, S. Zheng, and R. L. Frost, Int. J. Miner. Process. **125**, 18 (2013).
31. D. Liu, P. Yuan, D. Tan, H. Liu, T. Wang, M. Fan, J. Zhu, and H. He, J. Colloid Interface Sci. **388**, 176 (2012).
32. M. Li, N.M. Jahed, K. Min, and K. Matyjaszewski, Macromolecules **37**, 2434 (2004).
33. K. Khezri, RSC Adv. **6**, 109286 (2016).
34. A. Asfadeh, V. Haddadi-Asl, M. Salami-Kalajahi, M. Sarsabili, and H. Roghani-Mamaqani, Nano **8**, 1350018 (2013).
35. Y. Fazli and K. Khezri, Colloid Polym. Sci. (2016). doi 10.1007/s00396-016-3997-1
36. K. Khezri and Y. Fazli, High Temp. Mater. Proc. (2016). doi 10.1515/htmp-2015-0244
37. K. Khezri and H. Mahdavi, Z. Phys. Chem. **230**, 1499 (2016).
38. K. Khezri, and Y. Fazli, J. Inorg. Organomet. Polym. (2016). doi 10.1007/s10904-016-0469-5